

Aggregation Model and Market Mechanism for Virtual Power Plant Participation in Inertia and Primary Frequency Response

Changsen Feng, *Member, IEEE*, Zhongliang Huang, Jun Lin, Licheng Wang, Youbing Zhang, *Senior Member, IEEE*, and Fushuan Wen, *Fellow, IEEE*

Abstract-- The declining inertia provision from synchronous generators in modern power systems necessitates aggregating distributed energy resources (DERs) into virtual power plants (VPPs) to unlock their potential in delivering inertia and primary frequency response (IPFR) through ancillary service markets. To facilitate DER participation in the IPFR market, this paper proposes a DER aggregation model and market mechanism for VPP participating in IPFR. First, an energy-IPFR market framework is developed, in which a VPP acts as an intermediary to coordinate heterogeneous DERs. Second, by taking into account the delay associated with inertia, an optimization-based VPP aggregation method is introduced to encapsulate the IPFR process involving a variety of DERs. Third, an energy-IPFR market mechanism with VPP participation is introduced, aiming to minimize social costs while considering the frequency response delay characteristics of the participants. Finally, the performance of the proposed approaches is verified by case studies on a modified IEEE 30-bus system.

Index Terms-- Virtual power plants, frequency response aggregation, time delay, inertial response, primary frequency response, market mechanism.

NOMENCLATURE

A. Acronyms

| | |
|-------|--|
| EV | Electric vehicle |
| FL | Flexible load |
| GFM | Grid-forming |
| IPFR | Inertia and primary frequency response |
| QSS | Quasi-steady-state |
| PFR | Primary frequency response |
| PWL | Piecewise linearization |
| REG | Renewable energy generator |
| RoCoF | Rate-of-change-of-frequency |
| SG | Synchronous generator |
| VPP | Virtual power plant |

B. Index

| | |
|---------------|-------------------------------|
| ν, ω | Index of VPP aggregated order |
|---------------|-------------------------------|

| | |
|---|--|
| hp | Index of PWL planes |
| i, j, k, l | Index of SGs, GFM REGs, GFM energy storage, VPPs |
| n, m | Index of buses in the system |
| ν | Index of internal units within VPP |
| C. Sets | |
| $\Omega_{G/ESS/REG/VPP}$ | Set of SGs/energy storage/REGs/VPPs in the system |
| $N_{G/FM}$ | Set of SGs/others within the VPP |
| N_{hp} | Set of PWL planes |
| D. Parameters | |
| $\alpha_{i/j/k,t}^{G/REG/ESS}$ | Unit power generation costs of SG i /REGs j /energy storage k at time t |
| $\alpha_{l,t}^{VPPG} \alpha_{l,t}^{VPPR}$ | Unit power generation costs of internal SGs and other parts of VPP l at time t |
| $\beta_{j/k/l,t}^{REG/ESS/VPPR}$ | Unit virtual inertia costs of REGs j /energy storage k / VPP l at time t |
| $\lambda_{j/k/l,t}^{REG/ESS/VPP}$ | Unit droop factor costs of REGs j /GFM energy storage k / VPP l |
| $\rho_{i/j/k/l,t}^{G/REG/ESS/VPP.EN}$ | Price of SG i / REG j / energy storage k / VPP l providing unit power at time t |
| $\rho_{i/j/k/l,t}^{G/REG/ESS/VPP.IN}$ | Price of SG i / REG j / energy storage k / VPP l providing unit inertia at time t |
| $\rho_{i/j/k/l,t}^{G/REG/ESS/VPP.DF}$ | Price of SG i / REG j / energy storage k / VPP l providing unit droop factor at time t |
| κ_{ν} | Equivalent gain of internal unit ν |
| κ_{hp} | Parameter of PWL planes |
| λ_{ν} | Normalized gain of feedback loop in frequency response model of unit ν |
| $\lambda_{nadir}, \lambda_{qss}$ | Penalty coefficients for the nadir frequency and QSS frequency |
| τ_1, τ_2 | Time delay of GFM power equipment IPFR, SG PFR |
| Φ_A | Constant coefficient of operational power for the FL |
| $C(s)$ | Thermodynamic equivalent constant of the FL compressor |
| ΔD | System disturbance value |
| D_G | Damping of the small SG |
| $\Delta f_{nadir-max}^f$ | Maximum boundary for ensuring the security of the system nadir frequency |
| $\Delta f_{qss}^{e,ref}$ | Maximum boundary for QSS frequency deviation |

This work is supported by National Natural Science Foundation of China (No. 52107129 and U22B20116).

C. Feng, Z. Huang, J. Lin, L. Wang and Y. Zhang are with College of Information Engineering, Zhejiang University of Technology, Hangzhou 310023, China (e-mail: fcs@zjut.edu.cn, 201906080109@zjut.edu.cn, 211122030080@zjut.edu.cn, wanglicheng@zjut.edu.cn, youbingzhang@zjut.edu.cn).

F. Wen is with the School of Electrical Engineering, Zhejiang University, Hangzhou 310027, China, and F. Wen is also with the Hainan Institute, Zhejiang University, Sanya 572000, China (e-mail: fushuan.wen@gmail.com).

| | |
|--|---|
| F_H | Power ratio of the high-pressure cylinder |
| $G_{VPP}(s)$ | Aggregate transfer function of VPP PFR |
| $H_{G/FM}$ | (Virtual) Inertia of small SG/GFM power equipment within VPP |
| $H_{VPPG/VPPR}$ | Non-delayed/delayed inertia provided by small SGs/GFM power equipment |
| $k_{G/FM/EV/FL/VPP}$ | Droop factor of small SG/GFM power equipment/EV/FL/VPP |
| k_v, h_ω | v, ω order coefficients of the numerator and denominator in the polynomial |
| $K_{m,v}$ | Capacity proportion of unit v within VPP |
| $P_{i,t,\min}^{G,EN}, P_{i,t,\max}^{G,EN}$ | Minimum and maximum generated active power of SG i in time period t |
| $P_{i/l}^{Ramp}$ | Maximum ramping rate of SG i /small SG in VPP l |
| $P_{l,t,\min}^{VPP/VPPR,IN/VPP,DF}$ | Minimum of full capacity/reserve capacity for providing virtual inertia/droop factor of VPP l |
| $P_{l,t,\max}^{VPP/VPPR,IN/VPP,DF}$ | Maximum full capacity/reserve capacity for providing virtual inertia/droop factor of VPP l |
| $RoCoF_{\max}$ | Maximum boundary of RoCoF |
| T_G, T_R, T_C | Time constants of the governor, reheater, steam volume of small SGs |
| $T_{FM/EV/FL/A}$ | Time constant of the GFM inverter response/EV charging/FL compressor/FL thermodynamic |

E. Variables

| | |
|--|--|
| $\theta_{n,t}$ | Angle of node n at time t |
| $B_{n,m}$ | Admittance between nodes n and m |
| $D_{n,t}$ | Power load of node n at time t |
| $\Delta f(t), f(t)$ | Function of system frequency using the detailed or equivalent VPP model |
| $H^{TO/GV}$ | Total inertia/non-delay inertia of the system |
| $H_{i/l,t}^{G/VPPG}$ | Non-delay inertia provided by SG i / VPP l at time t |
| $H_{j/k/l,t}^{REG/ESS/VPPR}$ | Virtual inertia provided by REG j /energy storage k / VPP l at time t |
| $k_{i/j/k/l,t}^{G/REG/ESS/VPP}$ | Droop factor provided by SG i / REG j /energy storage k / VPP l at time t |
| $\Delta P_{i/j/k/l,t}^{G/REG/ESS/VPP}$ | Energy power increment of SG i / REG j /energy storage k / VPP l at time t |
| $P_{i/j/k,t}^{G/REG,EN/ESS,EN}$ | Energy power provided by SG i / REG j /energy storage k at time t |
| $P_{l,t}^{VPPG/VPPR,EN}$ | Energy power provided by SG part/rest part of the VPP l at time t |
| t_{nadir}, t_{nadir}^* | Times at which the system frequency reaches the nadir before and after the equivalent transfer function is adopted |
| $x_{i/l,t}$ | Status of SG i /small SG portion of the VPP l indicating start-up/shut-down states at time t |
| $y_{i,t}^{SU/SD}$ | Status of SG i indicating start-up/shut-down actions at time t |

I. INTRODUCTION

IN modern power systems, the high penetration of renewable energy resources has led to a significant reduction in system inertia, increasing the risk of rapid frequency drop following system disturbances, which poses critical challenges to frequency stability [1], [2]. For instance, during the South Australian grid blackout in September 2016, the loss of 456 MW power generation within 8 seconds caused the frequency to drop to 47 Hz and the maximum rate-of-change-of-frequency (RoCoF) reaches 6.25 Hz/s, which is far beyond the system's frequency security boundary [3]. Similar events have been observed in other countries such as the United States [4] and the United Kingdom [5].

To address the challenges related to frequency security, it is essential to establish an effective ancillary market to support system frequency during large disturbances [6]. Inertia and primary frequency response (IPFR), as key components of ancillary services, play a vital role in mitigating frequency fluctuations within the first 30 seconds following a disturbance [7]. Designing a market mechanism for IPFR can incentivize frequency regulation resources to participate effectively, thereby alleviating the challenges caused by low inertia. Existing ancillary markets primarily focus on inertia response and primary frequency response (PFR). For example, EirGrid and National Grid Electricity System Operator (NGESO) currently purchase inertia as an ancillary service product [6]. Meanwhile, the Electric Reliability Council of Texas (ERCOT) is currently operating a PFR market [8] and the Australian Energy Market Operator (AEMC) is integrating PFR resources into contingency frequency services and promoting inertia participation in the ancillary market [9].

In existing research, researchers have explored market mechanisms from various perspectives. For instance, [10] presents a virtual inertia market mechanism for inverter-based power equipment while [11] introduces an inertia pricing scheme in a stochastic electricity market that includes various power devices providing (virtual) inertia. Similarly, the necessity of PFR markets is clarified in [12], and analytical methods are employed in [13] to develop PFR market mechanisms. To ensure fair settlement of PFR resources, [14] proposes a pricing mechanism consisting of two types of marginal prices for PFR, each with a different emphasizing aspect. However, these studies focus solely on either inertia or PFR. While in reality, inertia and PFR processes are strongly correlated. To address this issue, an IPFR market clearing mechanism based on synchronous generator (SG) response rates is proposed in [15] to quantify the effectiveness of frequency response. Furthermore, IPFR markets are further expanded by incorporating other distributed energy sources, considering their distinct frequency response characteristics, such as variable renewable energy generators (REGs) [16], energy storage [17], converter-interfaced generators [18], and inverter-based resources [19]. In addition, joint energy markets [16], unit delays [17], recovery effects [19], and other factors are also explored to enhance IPFR market mechanisms in these studies.

TABLE I

COMPARISON OF THE CONSIDERED FACTORS IN IPFR MARKET MECHANISM IN THE EXISTING LITERATURE AND THIS PAPER

| Refs. | Differen- tiated pricing | Joint energy market | REG participa- tion | Inertia delay | VPP participa- tion |
|------------------|--------------------------------|---------------------------|---------------------------|------------------|---------------------------|
| [10] | ✓ | × | ✓ | × | × |
| [11] | × | ✓ | ✓ | × | × |
| [12] | × | ✓ | × | × | × |
| [13], [15] | ✓ | ✓ | × | × | × |
| [14], [16], [18] | ✓ | ✓ | ✓ | × | × |
| [17], [19] | ✓ | ✓ | ✓ | ✓ | × |
| This paper | ✓ | ✓ | ✓ | ✓ | ✓ |

The market mechanisms for various resource entities participating in system IPFR are studied in the above-mentioned research. However, distributed energy resources (DERs) are unable to participate in the market individually due to their small capacities [20]. So, virtual power plants (VPPs) are employed to aggregate large numbers of DERs to enable them to participate in the IPFR market [21]. VPPs can leverage the flexibility and controllability of aggregated DERs to support system frequency [22]. Nevertheless, aggregating a large number of DERs significantly increases the number of frequency response parameters, which complicates market interactions [23]. This poses a critical challenge for designing IPFR market mechanisms for VPPs. Thus, it is essential to aggregate the frequency response parameters of DERs within VPPs and reduce the order of IPFR models, while maintaining the original accuracy.

Various equivalent aggregation models for VPP frequency responses have been proposed in recent studies, covering different DER types and scenarios. An analytical approach to consolidate the frequency response model of a multi-machine system into a single machine is presented in [24]. An equivalent aggregation model is derived in [25] based on the polynomial fitting of PFR characteristic curves of generator sets. To obtain a more accurate frequency dynamic aggregation model, DERs equivalent control loop is modeled [26], [27]. However, these methods mainly rely on fitting or weighted averaging methods, which may compromise the accuracy of security boundary estimation during system frequency responses. To address this limitation, [28] considers response delays among diverse DERs and aggregates transient frequency support parameters using an optimization framework. Additionally, a stepwise linear programming algorithm is employed in [29] to enhance the accuracy of frequency response aggregation models for feedback control branches of DERs. Nonetheless, the extensive heterogeneity of DERs is not adequately addressed in these approaches, a more robust equivalent aggregation model for VPP frequency responses in the IPFR market is still needed.

TABLE II
COMPARISON OF THE CONSIDERED FACTORS IN THE VPP AGGREGATION MODEL IN THE EXISTING LITERATURE AND THIS PAPER

| Refs. | Inertia aggrega- tion | PFR aggrega- tion | Optimi- zation method | Hetero- geneous response | Re- sponse delay |
|------------|-----------------------------|-------------------------|-----------------------------|--------------------------------|------------------------|
| [24], [25] | ✓ | ✓ | × | × | × |
| [26] | ✓ | ✓ | × | ✓ | × |
| [27] | × | ✓ | × | × | × |
| [28] | × | ✓ | ✓ | × | ✓ |
| [29] | ✓ | ✓ | ✓ | ✓ | × |
| This paper | ✓ | ✓ | ✓ | ✓ | ✓ |

To fill the above research gap, this paper proposes a novel VPP frequency response aggregation model. Based on the

model, we also develop an energy-IPFR joint market that incorporates the time delays of various DERs. The comparisons of the key features in the existing literature and our proposed methods are listed in Table I and Table II. The contributions of this paper are summarized as follows:

1) An IPFR market framework that incorporates VPPs and inertia delays is introduced. The framework details how the system operator (SO) facilitates the clearing of frequency regulation resources with diverse characteristics while enabling VPPs to optimally allocate heterogeneous DERs.

2) A VPP frequency response equivalent aggregation model is proposed to capture the IPFR dynamics of VPPs comprising various DER types. The model determines its parameters through weighted averaging and stochastic gradient descent methods, which effectively consider a wide range of inertia response delays of DERs. It succinctly and efficiently characterizes the IPFR effects of aggregated DERs using a minimal set of parameters.

3) Building on the inertia delay characteristics of various DER types in VPPs and the proposed VPP aggregation model, a joint energy-IPFR market mechanism is designed. This joint market mechanism allows SGs, grid-forming (GFM) power equipment, and VPPs to participate in bidding. We further establish a market clearing framework tailored to different market participants, thereby facilitating various resources participating in the IPFR market.

II. IPFR ANCILLARY SERVICES FRAMEWORK

In this section, we introduce the frequency-security boundaries of the system. Building on this foundation, we highlight the critical role of IPFR services for various resources. Considering the time delay associated with different resources and VPP participation, we propose an IPFR market framework for VPPs and their internal DERs participating in frequency response.

A. Ancillary Service for IPFR

When a power system experiences a contingency, it is essential to implement effective measures to restore the frequency to a steady state. To characterize the stability of the system following a disturbance, three critical boundaries are defined [30]: RoCoF maximum boundary $RoCoF_{max}$, frequency nadir deviation boundary $\Delta f_{nadir-max}$, quasi-steady-state (QSS) frequency deviation boundary Δf_{qss}^{ref} . They should satisfy certain conditions: $RoCoF_{max} < 0.125\text{Hz/s}$, $\Delta f_{nadir-max} < 0.05\text{Hz}$, $\Delta f_{qss}^{ref} < 0.025\text{Hz}$.

During system disturbances, the SO plays a crucial role. The SO facilitates several frequency services by dispatching various resources in the ancillary service market. As the low inertia issue in modern power systems becomes increasingly evident, the need increases for frequency ancillary service during the initial stages of disturbances, making IPFR even more critical.

In traditional power systems, the IPFR process following a disturbance can be derived from the physical characteristics of SGs. The IPFR process of the traditional power system consists of an inertial response and a PFR process. The inertia

response process is governed by the rotor swing equation of the SG:

$$2H_i^G \cdot \frac{d\Delta f(t)}{dt} = \Delta P_i^G - \Delta D, i \in \Omega_G \quad (1)$$

Additionally, the generator governor converts mechanical kinetic energy into electrical energy. The released electrical energy contributes to the fluctuations in PFR support frequency:

$$T_i^G \frac{d\Delta P_{i,t}^G}{dt} + \Delta P_{i,t}^G = -k_i^G \Delta f(t), i \in \Omega_G, t \geq \tau_2 \quad (2)$$

In addition, recently developed technologies such as VPPs and GFM can also participate in IPFR by adjusting virtual inertia and droop factors. The IPFR time dynamics of diverse resources are illustrated in Fig. 1. GFM power equipment must avoid frequent triggering of frequency responses within the anti-disturbance control loop design, resulting in a delay denoted as τ_1 . For SGs, due to the mechanical characteristics, there is a delay of τ_2 in the PFR process. Notably, VPPs can aggregate small SGs, which do not exhibit inertia response delays, along with power equipment capable of providing virtual inertia and droop factors thus enabling participation in frequency response throughout the entire IPFR market process.

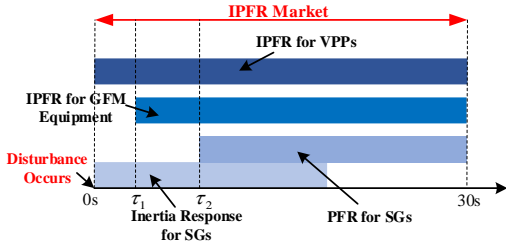


Fig. 1. The timeline of IPFR for different types of resources.

B. IPFR Market Framework with VPPs Participation

VPP aggregates various DERs and participates in auxiliary services as a single entity. Based on this, we propose a market framework that incorporates VPPs in the IPFR process, which is illustrated in Fig. 2.

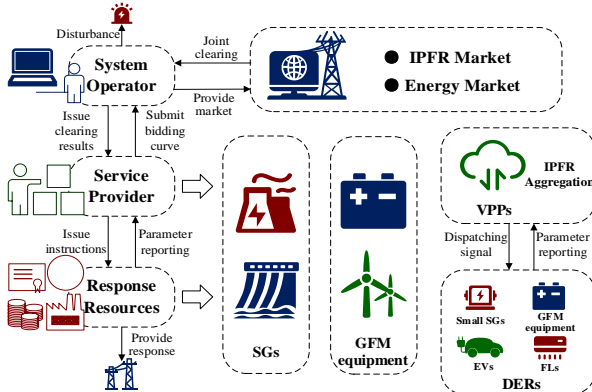


Fig. 2. Energy-IPFR joint market framework with VPPs participation.

In the IPFR market, participants are categorized into three main groups: SO, service providers, and response resources. Service providers submit to the SO the bidding curves for the energy market and the inertia/droop factor for the IPFR market. The SO then considers frequency-security constraints and the timeliness of inertia to clear the market. Following the market clearing results, the service provider sends control instructions

to the response resources.

Among the market participants, SGs and GFM power equipment act as both service providers and response resources. In contrast, VPPs serve solely as service providers. Prior to market opening, VPPs aggregate the IPFR process to generate the aggregated inertia and droop factor. Once the market opens, given the instantaneous requirements for inertia response in the clearing model, VPPs submit their bidding values for non-delay/delay inertia and the aggregated droop factor. After the market is cleared, VPPs match these results with the parameters of DERs to identify the mix of DERs that will provide services.

III. THE AGGREGATION MODEL OF VPP

In this section, we propose an aggregation model of various types of DERs in VPPs for the frequency response process, enabling their efficient participation in the IPFR market. First, taking into account the delay sensitivity of inertia, we aggregate delayed and non-delayed inertia separately based on the capacity ratios of different DERs. Next, we simplify the PFR process of homogeneous resources using an analytical approach. Finally, we aggregate the PFR process of heterogeneous resources using an optimization method.

A. Frequency Response Models of Multiple DERs

VPP aggregates a variety of adjustable DERs, including small SGs, GFM power equipment, electric vehicles (EVs), flexible loads (FLs), and other DERs that can provide inertia response or PFR.

The inertia response of small SGs is described (1) and the PFR of small SGs are derived from the governor of generators [31], as illustrated in Fig. 3.

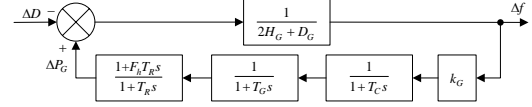


Fig. 3. IPFR model of small SGs speed regulator.

GFM power equipment achieves IPFR through inverter control. A common strategy is the virtual SG approach, which emulates SG rotor dynamics to provide virtual inertia and droop characteristics [32]. However, the inertia provided by GFM power equipment is associated with delay τ_1 as illustrated in Fig. 1. By incorporating a delay module, the IPFR model controlled by virtual SG is shown in Fig. 4. Notably, the response time constant of T_{FM} is extremely fast and is typically negligible.

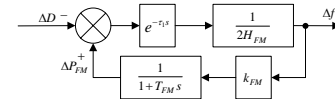


Fig. 4. IPFR model of GFM power equipment using VSG control.

Usually, several EVs are clustered as VPPs and connected to charging stations to provide potential system PFR [33]. The PFR model of VPPs of the EV cluster is shown in Fig. 5.

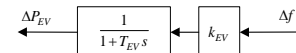


Fig. 5. Frequency response model of clusters of EVs.

Continuously adjustable FLs use converters or inverters to modulate power consumption by adjusting the working frequency of motors or compressors, a typical example of such

loads is inverter air conditioners [34]. This capability allows them to provide PFR, serving as the PFR model of adjustable FLs as illustrated in Fig. 6.

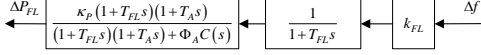


Fig. 6. Frequency response model of continuously adjustable FLs.

B. Frequency Response Aggregation of massive DERs

VPPs aggregate a diverse range of heterogeneous DERs. Based on the frequency response model in the last section, we first aggregate inertia response. The inertia response is primarily contributed by small SGs and GFM power equipment. To account for the inertia delay that significantly impacts the IPFR market, we categorize inertia into two types: non-delayed inertia which is provided by small SGs, and delayed inertia which is provided by GFM power equipment. The VPP's aggregate inertia time constant can be determined as follows:

$$\begin{cases} H_{VPPG} = \sum_{v \in N_G} H_{G,v} K_{m,v} \\ H_{VPPR} = \sum_{v \in N_{FM}} H_{FM,v} K_{m,v} \end{cases} \quad (3)$$

where $K_{m,v} = S_v / S_{sys}$ represents the ratio of the rated power of unit v to the total system power.

Next, we derive the equivalent aggregated PFR function for the massive number of DERs. Given the considerable number of units of each type of PFR resource, it is both computationally intensive and impractical to directly model a heterogeneous multi-machine frequency response model for the IPFR market. Therefore, it is necessary to aggregate the numerous homogeneous multi-machine frequency response model for the IPFR market. Therefore, it is necessary to aggregate the numerous homogeneous multi-machine DERs into an equivalent aggregation model.

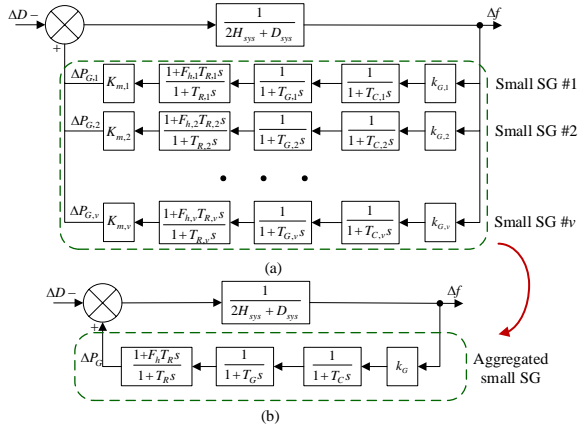


Fig. 7. Aggregated frequency response model of homogeneous machines.

For homogeneous DERs, the frequency response model is similar. We apply a weighted average method to aggregate the frequency response model. Taking small SGs as an example, Fig. 7 illustrates the process of aggregating the multi-machine model of a SG into a single-machine model.

In Fig. 7, the equivalent droop factor can be calculated as:

$$k_G = \sum_{v \in N_G} K_{m,v} k_{G,v} = K_G \sum_{v \in N_G} k_{G,v} = \sum_{v \in N_G} \kappa_v \quad (4)$$

where the equivalent gain is defined as $\kappa_v = K_{m,v} k_{G,v}$. In the aggregated frequency response model shown in Fig. 7(b), the equivalent parameters (T_R , T_G , T_C , F_h) represent the aggregated effect of multiple governors. To simplify the description, the normalized gain $\lambda_v = \kappa_v / k_G$ for each feedback loop is defined in

Fig. 7(a). By introducing λ_v , the homogeneous multi-machine transfer function model can be represented as a single-machine transfer function model, with the aggregated parameters below:

$$\begin{cases} T_h = \sum_{v \in N_G} \lambda_v T_{h,v}, T_R = \sum_{v \in N_G} \lambda_v T_{R,v} \\ T_s = \sum_{v \in N_G} \lambda_v T_{s,v}, F_h = \sum_{v \in N_G} \lambda_v F_{h,v} \end{cases} \quad (5)$$

The parameter simplification process and its theoretical proof are detailed in [24].

The parameters of the frequency response model can also be simplified using the weighted average method. Then, the frequency response model of the VPP can be aggregated into a unified heterogeneous multi-machine model, which is shown in Fig. 8(a).

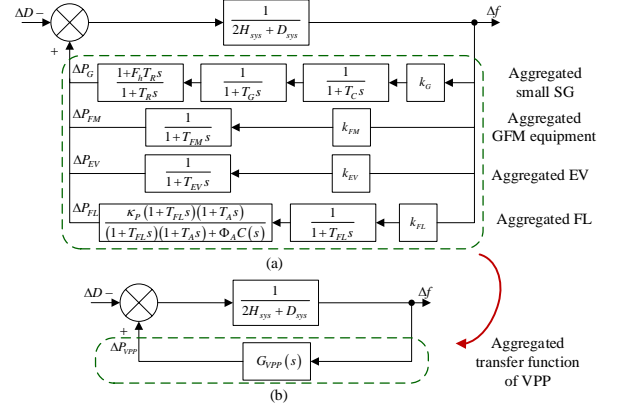


Fig. 8. Frequency response model of VPP considering multi-types of DERs.

Considering the timeliness and demands of the IPFR market, a single aggregated transfer function with a droop factor is proposed to effectively describe its complex PFR feedback loop, which can be expressed as follows:

$$G_{VPP}(s) = \frac{k_v s^v + k_{v-1} s^{v-1} + \dots + k^{VPP}}{h_\omega s^\omega + h_{\omega-1} s^{\omega-1} + \dots + h_1 s + 1} \quad (6)$$

As indicated in (6), when the polynomial order of the aggregated transfer function is low, the aggregated multi-machine model in Fig. 8(a) can be further simplified to a single digit, and the number of model parameters can be reduced from 20 to X.

C. Parameter Optimization of the VPP Aggregation Model

When aggregating the VPP equivalent frequency response model, it is essential to design an optimization method to derive the aggregated transfer function $G_{VPP}(s)$. In Section II-A, we outlined three frequency security boundaries. Among them, the frequency nadir f_{nadir} and the QSS frequency f_{qss} are crucial indicators of PFR capability. Therefore, when the system is subject to disturbances, it is critical to ensure that the errors in f_{nadir} and f_{qss} in the equivalent transfer function remain within acceptable limits. The equations for the PFR frequency security boundaries with the multi-machine feedback loop and the equivalent loop are shown in (7):

$$\begin{cases} f_{nadir} = f_0 + \Delta f(t_{nadir}), f_{qss} = f_0 + \Delta f(\infty) \\ f_{nadir} = f_0 + \Delta f(t_{nadir}^*), f_{qss} = f_0 + \Delta f(\infty) \end{cases} \quad (7)$$

Additionally, the initial disturbance is assumed to follow

the normal distribution provided by the SO. Then, the parameters of the VPP equivalent aggregation model can be determined by solving the following optimization problem (8)-(9):

$$\min_{\Delta D} \mathbb{E} \left[\left(\Delta f(t_{nadir}^*) - \Delta f(t_{nadir}) \right)^2 + \left(\Delta f(\infty) - \Delta f(\infty) \right)^2 \right] \quad (8)$$

$$\text{s.t.} \quad \begin{cases} \Delta f'(t_{nadir}) = 0, \Delta \tilde{f}'(t_{nadir}^*) = 0 \\ \Delta f'(\infty) = 0, \Delta \tilde{f}'(\infty) = 0 \end{cases} \quad (9)$$

Equation (8) aims to minimize the f_{nadir} and f_{qss} errors. Equation (9) is the constraint of the aggregated model and the multi-machine model. Specifically, that $RoCoF=0$ when the system frequency is f_{nadir} and f_{qss} .

However, (8)-(9) are nonlinearly constrained problems that are hard to solve, given that the parameters of the heterogeneous multi-machine model are known, and the frequency response curve of the model under disturbance can be calculated independently, the variable t_{nadir} can be treated as a known parameter. In addition, $\Delta f'(t_{nadir})$ can be seen as 0. So, we only need to design the penalty function by solving the optimization problem below:

$$\min_{\Delta D} \mathbb{E} \left[\left(\Delta f(t_{nadir}) - \Delta f(t_{nadir}) \right)^2 + \left(\Delta f(\infty) - \Delta f(\infty) \right)^2 \right] \quad (10)$$

$$+ \lambda_{nadir} \left\| \Delta \tilde{f}'(t_{nadir}) \right\|^2 + \lambda_{qss} \left\| \Delta \tilde{f}'(\infty) \right\|^2$$

In (10), the larger λ_{nadir} improves the accuracy of the timing of the f_{nadir} . Similarly, larger λ_{qss} will reduce the fluctuation of f_{qss} . The optimization problem (10) is thus a nonlinear unconstrained problem, which can be solved by the stochastic gradient descent algorithm [35].

IV. DYNAMIC FREQUENCY RESPONSE OF SYSTEM WITH VPP

In this section, we derive the multi-stage IPFR dynamic analytical formula, taking into account the delays associated with each service provider's IPFR characteristics. Then, by substituting the frequency security boundaries as the initial conditions into the formula, the frequency-security constraints of the system can be obtained.

A. IPFR Dynamics Considering Delay

In this paper, SGs, GFM power equipment, and VPPs are participants in the IPFR market. However, the characteristics of inertia and droop factor differ among different equipment, leading to distinct frequency response characteristics when engaging in the IPFR market. For SGs, The processes of IPFR are derived in (1), (2), and the relationship between the virtual inertia and droop factor provided by GFM power equipment has been discussed in Section III-A. In this context, T_{FM} can be considered negligible to simplify the derivation of frequency response expressions. The expressions are presented below:

$$\Delta P_k^{ESS} = -2H_k^{ESS} \frac{d\Delta f(t)}{dt} - k_k^{ESS} \cdot \Delta f(t), k \in \Omega_{ESS}, t \geq \tau_1 \quad (11)$$

$$\Delta P_j^{REG} = -2H_j^{REG} \frac{d\Delta f(t)}{dt} - k_j^{REG} \cdot \Delta f(t), j \in \Omega_{REG}, t \geq \tau_1 \quad (12)$$

VPP provides the derivation of the equivalent droop factor in detail in Section III. In this paper, we use the first-order model to represent the equivalent transfer function: $G_{VPP}(s) = k^{VPP} / (1 + T^{VPP}s)$. The accuracy of the first-order model

will be demonstrated by later case studies.

By applying the inverse Laplace transform to the VPP aggregation model, we obtain IPFR expressions as below:

$$\begin{cases} 2H_l^{VPPG} \cdot \frac{d\Delta f(t)}{dt} = \Delta P_l^{VPPR} - \Delta D, l \in \Omega_{VPP}, t < \tau_1 \\ 2H_l^{VPP} \cdot \frac{d\Delta f(t)}{dt} = \Delta P_l^{VPP} - \Delta D, l \in \Omega_{VPP}, t \geq \tau_1 \end{cases} \quad (13)$$

$$T_l^{VPP} \frac{d\Delta P_{t,l}^{VPP}}{dt} + \Delta P_{t,l}^{VPP} = -k_l^{VPP} \Delta f(t), l \in \Omega_{VPP} \quad (14)$$

Considering that power equipment exhibits different frequency response delays, the system frequency response process following a system disturbance (at $t=0^+$) should be divided into several stages:

Stage 1 ($0 \leq t < \tau_1$): The online independent SGs and the small SGs in the VPPs jointly provide inertia response.

Stage 2 ($\tau_1 < t \leq \tau_2$): GFM power equipment begins to provide virtual inertia and droop factor.

Stage 3 ($t > \tau_2$): The online SGs and the small SGs in the VPPs provide PFR for system stabilization.

Thus, the system dynamic frequency response can be expressed by (15), (16):

$$\begin{cases} 2H^{GV} \cdot \frac{d\Delta f(t)}{dt} = -\Delta D, 0 \leq t \leq \tau_1 \\ 2H^{GV} \cdot \frac{d\Delta f(t)}{dt} = \Delta P^{FM} + \Delta P^{VPPR} - \Delta D, \tau_1 < t \leq \tau_2 \\ 2H^{GV} \cdot \frac{d\Delta f(t)}{dt} = \Delta P^G + \Delta P^{FM} + \Delta P^{VPP} - \Delta D, t > \tau_2 \end{cases} \quad (15)$$

$$\begin{cases} H^{GV} = \sum_{i \in \Omega_G} x_{i,t} H_i^G + \sum_{l \in \Omega_{VPP}} x_{l,t} H_l^{VPPG} \\ H^{TO} = H^{GV} + \sum_{j \in \Omega_{REG}} H_j^{REG} + \sum_{k \in \Omega_{ESS}} H_k^{ESS} + \sum_{l \in \Omega_{VPP}} H_l^{VPPR} \\ \Delta P^{FM} = \sum_{k \in \Omega_{ESS}} \Delta P_k^{ESS} + \sum_{j \in \Omega_{REG}} \Delta P_j^{REG} \end{cases} \quad (16)$$

As shown in (16), the start-up/shut-down status of SGs influences the system inertia. SGs participating in the market are typically medium and large generators, of which the on/off time usually takes several hours. In contrast, VPP aggregates many small SGs with shorter on/off time of less than 1 hour [36], allowing their start-up/shut-down status to be modeled as continuous variables in the range of [0, 1]. This means that the VPP contributes to system inertia, and its participation in the IPFR market enhances the flexibility of the system's inertia response.

B. Frequency-security Constraints

Based on the multi-stage frequency response process, frequency-security constraints are established to determine the critical boundaries of system frequency security in Section II-A. When a disturbance occurs, the IPFR provided by GFM power equipment is subject to a delay τ_1 and does not participate in the inertia response. However, since the delay of IPFR from GFM power equipment is typically much smaller than that of SG PFR, it can be neglected when deriving frequency changes for $t > 0^+$. By combining (2) and (11)-(16) and substituting into the initial conditions $\Delta f|_{t=0^+} = 0$, the analytical for-

mula for the system frequency can be derived as (17):

$$\left\{ \begin{array}{l} \Delta f_1(t) = \frac{\Delta D}{2H^{GV}} t, \quad t=0^+ \\ \Delta f_2(t) = \frac{\Delta D}{k^{FM} + k^{VPPR}} \left(e^{-\frac{k^{FM} + k^{VPPR}}{2H^{TO}} t} - 1 \right), \quad 0^+ < t \leq \tau_2 \\ \Delta f_3(t) = \Delta D' e^{-\alpha t} [C_1 \sin(\omega t) + C_2 \cos(\omega t)] \\ \quad - \frac{\Delta D'}{k^G + k^{FM} + k^{VPP}}, \quad t > \tau_2 \end{array} \right. \quad (17)$$

where α , ω , $\Delta D'$, C_1 and C_2 are parameters of the dynamic frequency analytical formula, respectively. The derivation of the formula is detailed in Appendix.

Based on the analytical formula for system frequency dynamics, we can establish security constraints:

1) RoCoF constraint: $RoCoF_{\max}$ occurs immediately after the disturbance. By substituting $t=0^+$ into (17), we have:

$$RoCoF_{\max} \geq \frac{\Delta D}{2H^{GV}} \quad (18)$$

2) Frequency nadir constraint: Since $\Delta f_2(t)$ decreases monotonically, f_{nadir} occurs at $t > \tau_2$ when $\Delta f_3'(t_{\text{nadir}})=0$. The equation for frequency nadir constraint can be derived by substituting the initial conditions into (17). Since the frequency nadir constraint is nonlinear, it can be transformed into a linear constraint by piecewise linearization [16], as shown in (19):

$$\begin{aligned} \kappa_{hp}^1 H^{TO} + \kappa_{hp}^2 k^G + \kappa_{hp}^3 k^{FM} + \kappa_{hp}^4 k^{VPP} + \kappa_{hp}^5 \\ \geq -\Delta f_{\text{nadir-max}}, \quad hp \in N_{hp} \end{aligned} \quad (19)$$

3) QSS frequency constraint: By substituting $t \rightarrow \infty$ into (17), we can obtain the relaxed QSS constraint as follows:

$$\Delta f_{ss}^{\text{ref}} \geq \frac{\Delta D}{k^G + k^{FM} + k^{VPP}} \quad (20)$$

V. MARKET CLEARING MODEL

In this section, we design a joint market-clearing framework for electric energy and IPFR, incorporating the inertia and droop factor characteristics of different service providers. The clearing model considers the delays in inertia provided by various DERs within the VPP. Meanwhile, the droop factor and energy, which are not sensitive to delay, are cleared collectively by the VPP aggregation.

A. Framework for Solving Market Clearing Model

In the energy-IPFR joint market, it is essential to design a clearing model that captures different response characteristics of each participant. Given that the start-up/shut-down status of SGs is discrete, and their inertia and droop factors are coupled with electric energy, it is necessary to establish a security-constraint unit commitment (SCUC) model that accommodates these factors. Additionally, to satisfy the conditions of the strong duality theorem [12], a continuous SCUC model needs to be developed where the start-up/shut-down status is treated as continuous variables. In contrast, GFM power equipment allows for the decoupling of electric energy and inertia/droop factors. Subsequently, a security-constrained economic dispatch (SCED) model can be utilized to achieve market clearing. Furthermore, numerous small SGs within VPPs provide non-delayed inertia and collectively provide aggregated energy and droop responses. These contributions

can be modeled using the continuous SCUC and SCED frameworks to determine the clearing prices for inertia and energy/droop factor, respectively.

At first, the SCUC model is solved to obtain the unit commitment (UC) of SGs, while the inertia/droop factor clearing price for the SGs and the inertia clearing price for VPPs can be obtained by solving the continuous SCUC model. Subsequently, the SCED model is applied based on the UC results of SGs, allowing for the optimal allocation of electric energy, inertia, and droop factor across all types of service providers. This process ultimately determines the clearing price for GFM power equipment and the energy/droop factor clearing price for VPPs.

B. Objective Function of Clearing Model

The energy-IPFR joint market clearing model aims to minimize the social generation cost. The costs include electric energy cost, inertia cost, and droop factor cost, which are described by (21)-(24):

$$C^{TO} = \min \sum_{t=1}^{N_T} (c_t^{EN} + c_t^{IN} + c_t^{DF}) \Delta t \quad (21)$$

$$\begin{aligned} c_t^{EN} = \sum_{i \in \Omega_G} \alpha_{i,t}^G P_{i,t}^G + \sum_{j \in \Omega_{REG}} \alpha_{j,t}^{REG} P_{j,t}^{REG,EN} + \sum_{k \in \Omega_{ESS}} \alpha_{k,t}^{ESS} P_{k,t}^{ESS,EN} \\ + \sum_{l \in \Omega_{VPP}} (\alpha_{l,t}^{VPPG} P_{l,t}^{VPPG} + \alpha_{l,t}^{VPPR} P_{l,t}^{VPPR,EN}) \end{aligned} \quad (22)$$

$$c_t^{IN} = \sum_{j \in \Omega_{REG}} \beta_{j,t}^{REG} H_{j,t}^{REG} + \sum_{k \in \Omega_{ESS}} \beta_{k,t}^{ESS} H_{k,t}^{ESS} + \sum_{l \in \Omega_{VPP}} \beta_{l,t}^{VPPR} H_{l,t}^{VPPR} \quad (23)$$

$$c_t^{DF} = \sum_{j \in \Omega_{REG}} \chi_{j,t}^{REG} k_{j,t}^{REG} + \sum_{k \in \Omega_{ESS}} \chi_{k,t}^{ESS} k_{k,t}^{ESS} + \sum_{l \in \Omega_{VPP}} \chi_{l,t}^{VPP} k_{l,t}^{VPP} \quad (24)$$

C. Constraints of Clearing Model

The clearing model follows constraints, including power system constraints, SG operation constraints, VPP operation constraints, and GFM power equipment operation constraints.

1) Power System Constraints

$$\begin{aligned} \sum_{i \in \Omega_G} P_{i,t}^G + \sum_{j \in \Omega_{REG}} P_{j,t}^{REG,EN} + \sum_{k \in \Omega_{ESS}} P_{k,t}^{ESS,EN} + \sum_{l \in \Omega_{VPP}} P_{l,t}^{VPP,EN} \\ - \sum_{n \in \Omega_n} D_{n,t} - \sum_{m \in \Omega_n^N} B_{n,m} (\theta_{n,t} - \theta_{m,t}) = 0, \quad \forall n, \forall t: \lambda_{n,t}^{EN} \end{aligned} \quad (25)$$

$$H_t^{GV} \geq \frac{\Delta D}{2|RoCoF_{\max}|}, \quad \forall t: \lambda_t^{IN} \quad (26)$$

$$k_t^G + k_t^{FM} + k_t^{VPP} \geq \frac{\Delta D}{|\Delta f_{ss}^{\text{ref}}|}, \quad \forall t: \lambda_t^{DR} \quad (27)$$

$$\begin{aligned} \kappa_{hp}^1 H^{TO} + \kappa_{hp}^2 k^G + \kappa_{hp}^3 k^{FM} + \kappa_{hp}^4 k^{VPP} + \kappa_{hp}^5 \\ \geq -\Delta f_{\text{nadir-max}}, \quad hp \in N_{hp}, \quad \forall t: \lambda_t^{IPFR} \end{aligned} \quad (28)$$

Equation (25) represents the power balance constraint, while (26)-(28) outlining the frequency security constraints in Section IV-B. $\lambda_{n,t}^{EN}$, ν_t^{IN} , τ_t^{DR} , $\lambda_{hp,t}^{IPFR}$ are dual multipliers of (25)-(28).

2) SG Operating Constraints

$$x_{i,t} P_{i,t}^{G,EN} \leq P_{i,t}^G \leq x_{i,t} P_{i,t}^{G,EN}, \quad \forall i \in \Omega_G, \quad \forall t \quad (29)$$

$$-P_{i,t}^{\text{Ramp}} \leq P_{i,t}^G - P_{i,t-1}^G \leq P_{i,t}^{\text{Ramp}}, \quad \forall i \in \Omega_G, \quad \forall t \quad (30)$$

$$x_{i,t} - x_{i,t-1} = y_{i,t}^{SU} - y_{i,t}^{SD}, \quad \forall i \in \Omega_G, \quad \forall t \quad (31)$$

Equations (29)-(30) detail the output constraints and ramp-up constraints for SGs, respectively. Equation (31) specify the start-up/shut-down constraints for SGs.

3) VPP operation constraints

$$x_{i,t} K_G P_{l,t,\min}^{VPP} \leq P_{l,t}^{VPPG} \leq x_{i,t} K_G P_{l,t,\max}^{VPP}, \forall l \in \Omega_{VPP}, \forall t \quad (32)$$

$$-P_l^{Ramp} \leq P_{l,t}^{VPPG} - P_{l,t-1}^{VPPG} \leq P_l^{Ramp}, \forall l \in \Omega_{VPP}, \forall t \quad (33)$$

$$0 \leq P_{l,t}^{VPPR,EN} \leq (1 - K_G) P_{l,t,\max}^{VPP}, \forall l \in \Omega_{VPP}, \forall t \quad (34)$$

$$P_{l,\min}^{VPPR,IN} \leq 2 \underbrace{|\text{RoCoF}_{\max}| \cdot H_{l,t}^{VPPR}}_{P_{l,t}^{VPPR,IN}} \leq P_{l,\max}^{VPPR,IN}, \forall l \in \Omega_{VPP}, \forall t \quad (35)$$

$$P_{l,\min}^{VPP,DF} \leq \underbrace{(\Delta f_{\max-nadir} \cdot k_{l,t}^{VPP})}_{P_{l,t}^{VPP,DF}} \leq P_{l,\max}^{VPP,DF}, \forall l \in \Omega_{VPP}, \forall t \quad (36)$$

Equations (32)-(33) represent operation constraints for small SGs, while (34)-(35) denote operation constraints for other flexible resources. Equation (36) represent operation constraints when VPP l is considered as a whole entity.

It should be noted that the VPP participates in market clearing as an aggregate of DERs, and the operating constraints of various DERs cannot be fully captured. Therefore, the solution of different market-clearing models is categorized into two groups: SGs providing inertia and power equipment providing virtual inertia. If specific requirements arise for the VPP's participation in the market, the associated constraints can be sent to the SO prior to the clearing process.

4) GFM power equipment operation constraints

The operational constraints for GFM REG and GFM energy storage are the same for the SUCU, continuous SCUC, and SCED models [16], [17].

D. Pricing Mechanism of Joint Market

Based on the market clearing model, dual prices can be derived by the strong duality theorem, and a marginal cost pricing mechanism is employed to determine the prices of various services. In this framework, the market price of electric energy is represented by the dual multiplier $\lambda_{n,t}^{EN}$ associated with constraint (25). In addition, the prices for inertia and droop factors are established separately for each type of equipment.

For units that should be solved by continuous SCUC model, the inertia price, droop factor price of SG, and inertia price of VPP are derived by solving the dual constraints (26)-(28), resulting in (37)-(39):

$$\rho_{i,t}^{G,IN} = x_{i,t} \lambda_i^{IN} + x_{i,t} \sum_{hp \in N_{hp}} \kappa_{hp}^1 \lambda_{hp,t}^{IPFR} \quad (37)$$

$$\rho_{i,t}^{G,DR} = x_{i,t} \lambda_i^{DR} + x_{i,t} \sum_{hp \in N_{hp}} \kappa_{hp}^2 \lambda_{hp,t}^{IPFR} \quad (38)$$

$$\rho_{i,t}^{VPP,IN} = \lambda_{n,t}^{IN} + \sum_{hp \in N_{hp}} \kappa_{hp}^1 \lambda_{hp,t}^{IPFR} \quad (39)$$

For units that should be solved by the SCED model, the inertia price, droop factor price of GFM power equipment, and droop factor price of VPP are expressed as (40)-(42) by solving the dual constraints (27)-(28):

$$\rho_i^{FM,IN} = \sum_{hp \in N_{hp}} \kappa_{hp}^1 \lambda_{hp,t}^{IPFR} \quad (40)$$

$$\rho_i^{FM,DR} = \lambda_i^{DR} + \sum_{hp \in N_{hp}} \kappa_{hp}^3 \lambda_{hp,t}^{IPFR} \quad (41)$$

$$\rho_i^{VPP,DR} = \lambda_i^{DR} + \sum_{hp \in N_{hp}} \kappa_{hp}^4 \lambda_{hp,t}^{IPFR} \quad (42)$$

VI. CASE STUDIES

The performance of the proposed VPP aggregated model and joint market mechanism is verified in this section. The VPP frequency response aggregation model is built in MATLAB while the energy-IPFR market optimization problem is solved by the Gurobi solver in a Python environment.

Given the high proportion of renewable energy in modern power systems, a modified IEEE 30-bus system is utilized as a test system. In this model, the capacity of the independent SG, wind power, photovoltaic (PV), energy storage, and VPP are 260 MW, 110 MW, 320 MW, 50 MW, and 220 MW, respectively. The historical data of CAISO are used to generate a load curve, and the disturbance is set to 8% of the load value. The historical generation scenarios from CAISO data are selected to model REG uncertain outputs. The efficiency and initial state-of-charge of the energy storage is set as 0.95 and 0.5, respectively. There are totally three VPPs configured in this system. Detailed information regarding the DER types and their VPPs aggregated capacity are shown in Table III. The costs for different services of various resources are listed in Table IV, which are obtained from [16], [37].

TABLE III
TOTAL CAPACITIES OF DIFFERENT DER TYPES AGGREGATED BY VPPS

| VPP Number | Small SG | GFM Equipment | EV Clusters | Adjustable FLs |
|------------|----------|---------------|-------------|----------------|
| VPP #1 | 30 | 35 | 5 | 10 |
| VPP #2 | 26 | 18 | 10 | 8 |
| VPP #3 | 32 | 23 | 5 | 10 |
| Total | 88 | 76 | 20 | 28 |

TABLE IV
THE COSTS FOR DIFFERENT SERVICES OF VARIOUS PROVIDERS

| Provider | Service | Power (\$/MWh) | | Virtual Inertia (\$/(MW·s/Hz)) | Droop Factor (\$/(MW/Hz)) |
|----------------|---------|----------------|--------|--------------------------------|---------------------------|
| | | SG | Others | | |
| SG | | 30-35 | - | - | 0 |
| REG | | - | 4-6 | 2-4 | 3-5 |
| Energy Storage | | - | 12-16 | 2-4 | 3-5 |
| VPP | | 32-36 | 10-15 | 2-4 | 3-5 |

A. The Aggregation Model of VPP

Based on the proposed VPP frequency response equivalent aggregation method, first to third-order aggregation models are employed to equivalently represent the VPP frequency response process. The equivalent parameters obtained from the aggregation model are detailed in Table V.

TABLE V
EQUIVALENT PARAMETERS OF THE VPP AGGREGATION MODELS

| Parameters | Non-delayed Inertia (MW·s/Hz) | Delayed Inertia (MW·s/Hz) | Droop Factor (MW/Hz) |
|------------|-------------------------------|---------------------------|----------------------|
| VPP #1 | 4.1 | 3.3 | 19.5 |
| VPP #2 | 3.8 | 3.0 | 16.8 |
| VPP #3 | 4.3 | 3.1 | 17.5 |

The results of the system dynamic are shown in Fig 9. For VPP #1, we assume that all frequency regulation resources in the system are online, and the disturbance is set to normal distribution $X \sim N(80,12)$ MW when $t=0^+$. Also in Fig. 9, the second-order and third-order aggregation models demonstrate the advantage in capturing the frequency response, with f_{nadir} and f_{qss} values falling within the 95% confidence interval (CI) of the full-order frequency response model. The deviation values of first-order aggregation models are all less than 0.0003 p.u at 50 Hz reference frequency, which demonstrates high accuracy. Additionally, the frequency response curve of the first-order model is lower than that of the full-order model, which demonstrates that the result of the first-order method is con-

servative. Consequently, the proposed VPP aggregation model provides high accuracy in representing the IPFR process of the VPP.

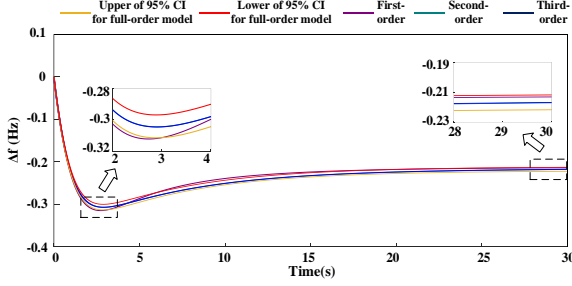


Fig. 9. System frequency response results using the different aggregation models of VPP #1.

Next, we examine the influence of inertia response delay in the aggregation model. A total of 500 scenarios are generated by assuming the disturbance follows the normal distribution. The results of the mean absolute percentage errors (MAPEs) of f_{nadir} and f_{qss} are demonstrated in Table VI.

TABLE VI

MAPEs of NADIR FREQUENCY AND QSS FREQUENCY USING MODELS WITH AND WITHOUT CONSIDERING DELAY

| Model Indicator | With Considering Delay | | | Without Considering Delay | | |
|----------------------------|------------------------|---------|---------|---------------------------|---------|---------|
| | 1-order | 2-order | 3-order | 1-order | 2-order | 3-order |
| MAPE of f_{nadir} | 2.38% | 0.10% | 0.12% | 2.56% | 0.10% | 0.13% |
| MAPE of f_{qss} | 1.49% | 0.11% | 0.03% | 1.67% | 0.14% | 0.03% |

As shown in Table VI, the results considering delay are only slightly better than those without. This is because the VPP aggregation model aggregates PFR through optimization, and the common objective function (10) results in little differences between the two models at f_{nadir} , f_{qss} . However, neglecting the inertia delay can lead to equivalent droop factor distortion, due to the sensitivity of inertia delay. Therefore, the VPP aggregation model that does not account for inertia delay is not suitable for the IPFR market.

In the spot market, the real-time settlement cycle is approximately 15 minutes [38], which poses strict time requirements for aggregating VPP frequency response parameters. In our simulation, the calculation time for the first, second, and third-order models is 87, 61, and 37 seconds, respectively, which satisfy the time requirements for electric market bidding.

B. Market Clearing Results

In the IPFR energy market, the clearing results of each power equipment are illustrated in Fig. 10. In Fig. 10(a), due to the high proportion of VPPs in the system, when REG output is low (0-7h and 19-23h), VPPs serve as more cost-effective energy suppliers compared to SGs. By contrast, when REG output is sufficient (8-18h), REGs are prioritized for energy provision. The fluctuations in electric energy prices are shown in Fig. 10(b). Due to the relatively uniform distribution of various types of During the 0-6h and 20-23h, the absence of PV generation limits the system's ability to meet high demand, leading to a sharp increase in electricity prices.

In the IPFR market, the inertia and droop factor clearing results are illustrated in Fig. 11 and Fig. 12, respectively.

In Fig. 11(a), inertia is provided solely by SGs and VPPs, this is due to the system's highest demand for inertia occurring immediately following a disturbance. The SGs and VPPs can provide non-delay inertia to support the system frequency. Additionally, the flexibility of these small SGs in the VPP

effectively compensates for the system's decreasing inertia, and the frequent start-up/shut-down of independent SGs can be reduced. Fig. 11(b) displays the clearing price of inertia. The high inertia price is caused by significant disturbances in the system and shortage of inertia, particularly due to the high proportion of renewable energy resources.

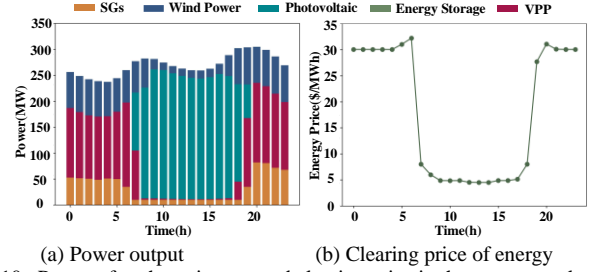


Fig. 10. Power of each equipment and clearing price in the energy market.

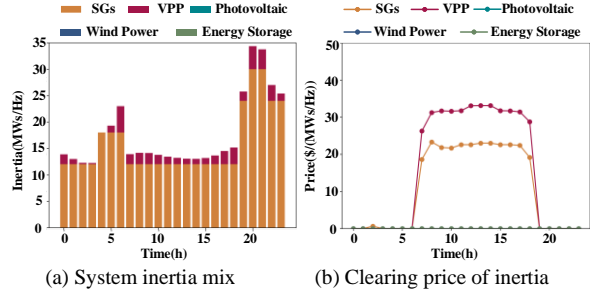


Fig. 11. System inertia mix and inertia clearing price.

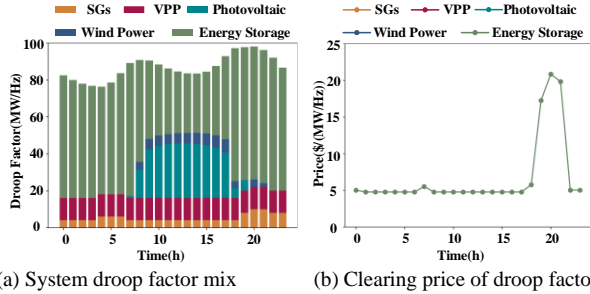


Fig. 12. System droop factor mix and droop factor clearing price.

Fig. 12(a) presents the results of the droop factor of the system. Due to the high cost of power generation from energy storage, it is typically not the preferred option in the energy market. However, its flexibility makes it highly effective in meeting the droop factor requirements in the IPFR market. Consequently, energy storage equipment provides the majority of the droop factors in the system. Additionally, VPPs consistently provide droop factors thanks to their low costs and high dispatchability. As shown in Fig. 12(b), the droop factor clearing price remains relatively stable most of the time, with a significant increase happening between 19-21h. This is due to a shortage of system inertia and droop factors, requiring the activation of additional SGs. The small generation limits of these SGs constrain the output of marginal units, pushing up operating costs and triggering a sharp rise in prices.

C. Benefits of the VPP Participation

To demonstrate the benefits of VPP participation in the energy-IPFR market, we design two comparative scenarios. Scenario 1 utilizes the basic system introduced in this case study, while Scenario 2 involves shutting down all VPPs and proportionally increasing the capacity of other resources. The costs and net profits of these two scenarios are presented in Table VII.

TABLE VII
COST AND NET PROFIT OF JOINT MARKET WITH AND WITHOUT VPPS

| Service Provider | Scenario 1 | | Scenario 2 | |
|--------------------|------------|----------------|------------|----------------|
| | Cost(\$) | Net Profit(\$) | Cost(\$) | Net Profit(\$) |
| SG | 24679 | 615 | 70829 | -3062 |
| VPP | 19836 | 32973 | - | - |
| GFM REG | 17578 | 27020 | 19140 | 35319 |
| GFM energy storage | 6165 | 3430 | 5305 | 390 |
| Total | 68258 | 64038 | 95274 | 32647 |

For Scenario 1, VPPs have achieved substantial returns, indicating that the proposed market mechanism successfully incentivizes their participation in the system's IPFR process. The comparison between Scenario 1 and Scenario 2 demonstrates that the integration of VPPs into the energy-IPFR joint market enhances the system's flexibility in energy and inertia provision, leading to reduced total costs and improved net profits. In addition, the price of inertia increases due to a smaller proportion of inertia-providing units in the system. Consequently, the net profit of SGs, which provide significant non-delay inertia, is significantly improved. In conclusion, the simulation results demonstrate that the VPP frequency response aggregation model is well-suited for the power market. In low-inertia systems, VPPs optimize resource utilization, reduce frequency regulation costs, and improve overall system frequency security.

VII. CONCLUSION

A novel VPP aggregated model and a joint energy-IPFR market mechanism are proposed in this paper to address frequency stability challenges in low-inertia power systems. An optimization-based model that aggregates heterogeneous DERs is established. The dynamic formula that accounts for IPFR delay of various resources is used to derive frequency-security constraints. The energy-IPFR market mechanism is designed to facilitate various resources to participate in providing IPFR product. Numerical results validate the effectiveness of the VPP aggregated model, and demonstrate that the energy-IPFR market mechanism successfully facilitates DERs participation and fully leverages the advantages of VPPs in providing schedulable non-delay inertia.

APPENDIX

The derivation of (17) as follows:

Substituting (1),(13) into (15)-(16) yields (A-1), obtain:

$$2H^{GV} \frac{d\Delta f_1(t)}{dt} = -\Delta D, 0 < t \leq \tau_1 \quad (\text{A-1})$$

$\Delta f_1(t)$ can be obtained by substitute $\Delta f_1(0) = 0$ into (A-1).

We have discussed the feasibility of neglecting τ_1 when solving $\Delta f_2(t)$ in Section III-A. Consequently, substituting (11)-(12) into (15)-(16) yield (A-2). Its general solution is shown in (A-3). By substituting the $\Delta f_2(0) = 0$, $\Delta f_2(t)$ for $0 < t \leq \tau_2$ we have (A-4).

$$\begin{cases} 2H^{TO} \frac{d\Delta f_1(t)}{dt} + (k^{FM} + k^{VPPR}) \Delta f_1(t) = -\Delta D, 0 < t \leq \tau_2 \\ k^{FM} = \sum_{k \in \Omega_{ESS}} k_k^{ESS} + \sum_{j \in \Omega_{REG}} k_j^{REG}, k^{VPPR} = \sum_{l \in \Omega_{VPP}} k_l^{VPPR} \end{cases} \quad (\text{A-2})$$

$$\begin{aligned} \Delta f_2(t) &= e^{-\int \frac{k^{FM} + k^{VPPR}}{2H^{TO}} dt} \left(C + \int -\frac{\Delta D}{2H^{TO}} e^{\int \frac{k^{FM} + k^{VPPR}}{2H^{TO}} dt} dt \right) \\ &= -\frac{\Delta D}{k^{FM} + k^{VPPR}} + C e^{\frac{k^{FM} + k^{VPPR}}{2H^{TO}} t}, 0 < t \leq \tau_2 \end{aligned} \quad (\text{A-3})$$

$$\Delta f_2(t) = \frac{\Delta D}{k^{FM} + k^{VPPR}} (e^{-\frac{k^{FM} + k^{VPPR}}{2H^{TO}} t} - 1), 0 < t \leq \tau_2 \quad (\text{A-4})$$

During the period $0 < t \leq \tau_2$, the GFM power equipment, and VPP have already provided a portion of the power ΔP_τ to the system. At $t = \tau_2$, the power deficiency $\Delta D' < \Delta D$ is present. The calculations for ΔP_τ and $\Delta D'$ are derived in (A-5)-(A-6).

$$\begin{aligned} \Delta P_\tau &= -2(H^{FM} + H^{VPPR}) \Delta f_2'(t) - (k^{FM} + k^{VPPR}) \Delta f_2(t) \Big|_{t=\tau_2} \\ &= \Delta D \left(1 - \frac{H^{GV}}{H^{TO}} e^{-\frac{k^{FM} + k^{VPPR}}{2H^{TO}} \tau_2} \right) \end{aligned} \quad (\text{A-5})$$

$$\Delta D' = \Delta D - \Delta P_\tau = \frac{H^{GV}}{H^{TO}} e^{-\frac{k^{FM} + k^{VPPR}}{2H^{TO}} \tau_2} \Delta D \quad (\text{A-6})$$

Substituting (1),(11)-(13) into (15)-(16) results in:

$$\begin{aligned} -\Delta D' &= 2H^{TO} T^{GV} \frac{d^2 \Delta f_3(t)}{dt^2} \\ &+ (2H^{GV} + k^{FM} T^{GV} + k^{VPP} T^{GV}) \frac{d\Delta f_3(t)}{dt} \\ &+ (k^G + k^{FM} + k^{VPP}) \Delta f_3(t) \end{aligned} \quad (\text{A-7})$$

$$\begin{cases} T^{GV} = \sum_{i \in \Omega_G} \lambda_i T_i^G + \sum_{l \in \Omega_{VPP}} \lambda_l T_l^{VPP} \\ k^G = \sum_{i \in \Omega_G} x_{i,t} k_i^G, k^{VPP} = k^{VPPR} + \sum_{l \in \Omega_{VPP}} x_{l,t} k_l^{VPPG} \end{cases} \quad (\text{A-8})$$

Solving (A-7), we get (A-9)-(A-11). By substituting the general solution into (A-12), we obtain (A-13). Notably, T_{GV} is the equivalent time constant of SG combined with VPP, solving it by the aggregation method proposed in Section III-B.

$$\begin{aligned} r_{1,2} &= -\frac{2H^{GV} + (k^{FM} + k^{VPP}) T^{GV}}{4H^{TO} T^{GV}} \\ &\pm \sqrt{\left(\frac{2H^{GV} + k^{FM} T^{GV} + k^{VPP} T^{GV}}{4H^{TO} T^{GV}} \right)^2 - \frac{k^G + k^{FM} + k^{VPP}}{2H^{TO} T^{GV}}} \end{aligned} \quad (\text{A-9})$$

$$\Delta f_3^*(t) = -\frac{\Delta D'}{k^G + k^{FM} + k^{VPP}} \quad (\text{A-10})$$

$$\begin{cases} \Delta f_3(t) = \Delta D' e^{-\alpha t} [C_1 \sin(\omega t) + C_2 \cos(\omega t)] \\ \alpha = \frac{2H^{TO} + (k^{FM} + k^{VPP}) T^{GV}}{4T^{GV} H^{TO}} \\ \omega = \sqrt{\frac{k^G + k^{FM} + k^{VPP}}{2T^{GV} H^{TO}} - \alpha^2} \end{cases} \quad (\text{A-11})$$

$$\begin{cases} \Delta f_2(t) \Big|_{t=\tau_2} = \Delta f_3(t) \Big|_{t=\tau_2^+} \\ \frac{d\Delta f_2(t)}{dt} \Big|_{t=\tau_2} = \frac{d\Delta f_3(t)}{dt} \Big|_{t=\tau_2^+} \end{cases} \quad (\text{A-12})$$

$$\left\{ \begin{aligned} & \frac{\Delta D}{k^{FM} + k^{VPP}} \left(e^{-\frac{k^{FM} + k^{VPP}}{2H^{TO}} \tau_2} - 1 \right) = - \frac{\Delta D'}{k^G + k^{FM} + k^{VPP}} \\ & \quad + \Delta D' e^{-\alpha \tau_2} [C_1 \sin(\omega \tau_2) + C_2 \cos(\omega \tau_2)] \\ & - \frac{\Delta D}{2H^{TO}} e^{-\frac{k^{FM} + k^{VPP}}{2H^{TO}} \tau_2} = \Delta D' e^{-\alpha \tau_2} [C_1 \omega \cos(\omega \tau_2) - C_2 \omega \sin(\omega \tau_2)] \\ & \quad - \Delta D' \alpha e^{-\alpha \tau_2} [C_1 \sin(\omega \tau_2) + C_2 \cos(\omega \tau_2)] \end{aligned} \right. \quad (A-13)$$

Obviously, $\Delta f_3(t)$ decreases monotonically, thereby the f_{nadir} occurs during $t > \tau_2$. Solving $\Delta f_3'(t)=0$, obtained:

$$\begin{aligned} \Delta f_2(t) &= \Delta D' e^{-\alpha t} [C_1 \sin(\omega t) + C_2 \cos(\omega t)] - \frac{\Delta D'}{k^G + k^{FM} + k^{VPP}} \\ &= \Delta D' e^{-\alpha t} [\sqrt{C_1^2 + C_2^2} \sin(\omega t + \varphi)] - \frac{\Delta D'}{k^G + k^{FM} + k^{VPP}} \end{aligned} \quad (A-14)$$

$$\begin{aligned} \Delta f_2'(t) &= \Delta D' e^{-\alpha t} \sqrt{C_1^2 + C_2^2} \omega \cos(\omega t + \varphi) \\ &\quad - \Delta D' e^{-\alpha t} \sqrt{C_1^2 + C_2^2} \alpha \sin(\omega t + \varphi) = 0 \end{aligned} \quad (A-15)$$

$$\left\{ \begin{aligned} & \sqrt{\alpha^2 + \omega^2} \sin(\omega t + \varphi + \varphi') = 0 \\ & \varphi' = \arctan \frac{\omega}{-\alpha} \end{aligned} \right. \quad (A-16)$$

$$t_{nadir} = - \frac{\varphi + \varphi'}{\omega} \quad (A-17)$$

REFERENCES

- [1] K. Yan, G. Li, R. Zhang, Y. Xu, T. Jiang, and X. Li, "Frequency control and optimal operation of low-inertia power systems with HVDC and Renewable Energy: A Review," *IEEE Trans. Power Syst.*, vol. 39, no. 2, pp. 4279-4295, Mar. 2024.
- [2] H. Alsharif, M. Jalili, and K. N. Hasan, "Fast frequency response services in low inertia power systems-A review," *Energy Reports*, vol. 9, pp. 228-237, Oct. 2023.
- [3] A. E. M. Operator, "Update report: black system event in South Australia on 28 September 2016," 2016.
- [4] G. Zhang, H. Zhong, Z. Tan, T. Cheng, Q. Xia, and C. Kang, "Texas electric power crisis of 2021 warns of a new blackout mechanism," *CSEE J Power Energy*, vol. 8, no. 1, pp. 1-9, Jan. 2022.
- [5] NGENSO, Technical Report on the events of 9 August 2019, 6 September 2019 [Online], 2021, [Accessed 6/8/2021], Available: [National Grid ESO LFDD 09/08/2019 Incident Report](https://www.neso.gov.au/~/media/NGESO/Reports/2021-09-08-2019-incident-report.pdf).
- [6] J. G. Zhou, Y. Guo, L. Yang, J. T. Shi, Y. Zhang, Y. S. Li, Q. L. Guo, and H. B. Sun, "A review on frequency management for low-inertia power systems: From inertia and fast frequency response perspectives," *Electr Pow Syst Res*, vol. 228, Mar. 2024.
- [7] F. Milano, F. Dörfler, G. Hug, D. J. Hill, and G. Verbic, "Foundations and challenges of low-inertia systems," *2018 Power Systems Computation Conference (Psc)*, 2018.
- [8] P. Du, N. V. Mago, W. Li, S. Sharma, Q. Hu, and T. Ding, "New ancillary service market for ERCOT," *IEEE Access*, vol. 8, pp. 178391-178401, 2020.
- [9] A. E. M. Operator, "Market ancillary service specification", 2022, Available: [Market Ancillary Services Specification - v7.0 effective 1 Feb 2021 - clean](https://www.aemo.com.au/~/media/Market%20Services/2022-02-01/Market-Ancillary-Services-Specification-v7.0-effective-1-Feb-2021-clean.pdf).
- [10] B. K. Poolla, S. Bolognani, N. Li, and F. Dörfler, "A market mechanism for virtual inertia," *IEEE Trans. Smart Grid*, vol. 11, no. 4, pp. 3570-3579, Jul. 2020.
- [11] Z. Liang, R. Mieth, and Y. Dvorkin, "Inertia pricing in stochastic electricity markets," *IEEE Trans. Power Syst.*, vol. 38, no. 3, pp. 2071-2084, May. 2023.
- [12] E. Ela, V. Gevorgian, A. Tuohy, B. Kirby, M. Milligan, and M. O'Malley, "Market designs for the primary frequency response ancillary service-Part I: Motivation and design," *IEEE Trans. Power Syst.*, vol. 29, no. 1, pp. 421-431, Jan. 2014.
- [13] G. Y. Zhang, E. Ela, and Q. Wang, "Market scheduling and pricing for primary and secondary frequency reserve," *IEEE Trans. Power Syst.*, vol. 34, no. 4, pp. 2914-2924, Jul. 2019.
- [14] K. Li, L. Wei, J. Fang, X. Ai, S. Cui, M. Zhu, and J. Wen, "Incentive-compatible primary frequency response ancillary service market mechanism for incorporating diverse frequency support resources," *Energy*, vol. 306, Oct 15. 2024.
- [15] Y. Yang, J. C. H. Peng, and Z. Ye, "A market clearing mechanism considering primary frequency response rate," *IEEE Trans. Power Syst.*, vol. 36, no. 6, pp. 5952-5955, Nov. 2021.
- [16] K. Li, H. Guo, X. Fang, S. Liu, F. Teng, and Q. Chen, "Market mechanism design of inertia and primary frequency response with consideration of energy market," *IEEE Trans. Power Syst.*, vol. 38, no. 6, pp. 5701-5713, Nov. 2023.
- [17] L. Zhu, K. Dong, L. Tang, Z. Li, and J. Yu, "Joint optimal clearing model for electric energy, inertia and primary frequency response considering synchronous inertia and energy storage virtual inertia values," *Proceedings of the CSEE*, vol. 44, no. 19, pp. 7543-7555, Oct. 2024.
- [18] H. Liao, C. Yang, H. Gao, W. Liu, H. Xin, X. Tang, and J. Zhao, "Comprehensive-contribution-based primary frequency regulation market design for the converter-integrated power system," *IEEE Trans. Power Syst.*, vol. 39, no. 2, pp. 3825-3838, Mar. 2024.
- [19] L. Badesa, C. Matamala, Y. Zhou, and G. Strbac, "Assigning Shadow prices to synthetic inertia and frequency response reserves from renewable energy sources," *IEEE Trans. Sustain. Energy*, vol. 14, no. 1, pp. 12-26, Jan. 2023.
- [20] W. Chen, J. Qiu, J. Zhao, Q. Chai, and Z. Dong, "Bargaining game-based profit allocation of virtual power plant in frequency regulation market considering battery cycle life," *IEEE Trans. Smart Grid*, vol. 12, no. 4, pp. 2913-2928, Jul. 2021.
- [21] H. Gao, T. Jin, C. Feng, C. Li, Q. Chen, and C. Kang, "Review of virtual power plant operations: Resource coordination and multidimensional interaction," *Appl. Energy*, vol. 357, Mar. 2024.
- [22] D. Qiu, A. M. Baig, Y. Wang, L. Wang, C. Jiang, and G. Strbac, "Market design for ancillary service provisions of inertia and frequency response via virtual power plants: A non-convex bi-level optimisation approach," *Appl. Energy*, vol. 361, May. 2024.
- [23] Y. Xie, Y. Zhang, W. J. Lee, Z. Lin, and Y. A. Shamash, "Virtual power plants for grid resilience: A concise overview of research and applications," *IEEE/CAA J Automatic*, vol. 11, no. 2, pp. 329-343, Feb. 2024.
- [24] Q. Shi, F. Li, and H. Cui, "Analytical method to aggregate multi-machine SFR model with applications in power system dynamic studies," *IEEE Trans. Power Syst.*, vol. 33, no. 6, pp. 6355-6367, Nov. 2018.
- [25] L. Liu, W. Li, Y. Ba, J. Shen, C. Jin, and K. Wen, "An analytical model for frequency nadir prediction following a major disturbance," *IEEE Trans. Power Syst.*, vol. 35, no. 4, pp. 2527-2536, Jul. 2020.
- [26] J. Chen, M. Liu, and F. Milano, "Aggregated model of virtual power plants for transient frequency and voltage stability analysis," *IEEE Trans. Power Syst.*, vol. 36, no. 5, pp. 4366-4375, Sep. 2021.
- [27] F. Sanniti, R. Benato, and F. Milano, "Participation of DERs to the bottom-up power system frequency restoration processes," *IEEE Trans. Power Syst.*, vol. 38, no. 3, pp. 2630-2640, May. 2023.
- [28] C. Feng, Q. Chen, Y. Wang, P. Kong, H. Gao, and S. Chen, "Provision of contingency frequency services for virtual power plants with aggregated models," *IEEE Trans. Smart Grid*, vol. 14, no. 4, pp. 2798-2811, Jul. 2023.
- [29] Z. Shi, H. Zhu, H. Zhao, P. Wang, Y. Liang, K. Wang, J. Chen, X. Zheng, and H. Liu, "Parameter estimation method for virtual power plant frequency response model based on SLP," *Energies*, vol. 17, no. 13, Jul. 2024.
- [30] Z. Zhang, E. Du, F. Teng, N. Zhang, and C. Kang, "Modeling frequency dynamics in unit commitment with a high share of renewable energy," *IEEE Trans. Power Syst.*, vol. 35, no. 6, pp. 4383-4395, Nov. 2020.
- [31] P. M. Anderson, and M. Mirheydar, "A low-order system frequency response model," *IEEE Trans. Power Syst.*, vol. 5, no. 3, pp. 720-729, Aug. 1990.
- [32] Q. Hu, R. Han, X. Quan, Z. Wu, C. Tang, W. Li, and W. Wang, "Grid-forming inverter enabled virtual power plants with inertia support capability," *IEEE Trans. Smart Grid*, vol. 13, no. 5, pp. 4134-4143, Sep. 2022.
- [33] S. Izadkhast, P. Garcia-Gonzalez, P. Frias, L. Ramirez-Elizondo, and P. Bauer, "An aggregate model of plug-in electric vehicles including distribution network characteristics for primary frequency control," *IEEE Trans. Power Syst.*, vol. 31, no. 4, pp. 2987-2998, Jul. 2016.
- [34] H. Hui, Y. Ding, Y. Song, and S. Rahman, "Modeling and control of FLs for frequency regulation services considering compensation of communication latency and detection error," *Appl. Energy*, vol. 250, pp. 161-174, Sep 15. 2019.
- [35] H. Robbins, and S. Monro, "A stochastic approximation method," *The Annals of mathematical statistics*, pp. 400-407, 1951.
- [36] S. Mitra, L. G. Sun, and I. E. Grossmann, "Optimal scheduling of industrial combined heat and power plants under time-sensitive electricity prices," *Energy*, vol. 54, pp. 194-211, Jun 1. 2013.
- [37] Y. Liu, M. Li, H. Lian, X. Tang, C. Liu, and C. Jiang, "Optimal dispatch of virtual power plant using interval and deterministic combined optimization," *Int J Elec Power*, vol. 102, pp. 235-244, Nov. 2018.
- [38] CAISO, "California independent system operator corporation fifth replacement electronic tariff," 2019. [Online]. Available: <https://www.caiso.com/Documents/Section8-AncillaryServices-asof-Aug12-2019.pdf>.